Nano Research 2013, 6(3): 191–199
DOI 10.1007/s12274-013-0295-9
Research Article

ISSN 1998-0124
CN 11-5974/O4

Fast and reliable identification of atomically thin layers of $TaSe_2$ crystals

Andres Castellanos-Gomez[1] (✉), Efrén Navarro-Moratalla[2], Guillermo Mokry[3], Jorge Quereda[3], Elena Pinilla-Cienfuegos[2], Nicolás Agraït[3,4], Herre S. J. van der Zant[1], Eugenio Coronado[2], Gary A. Steele[1], and Gabino Rubio-Bollinger[3] (✉)

[1] *Kavli Institute of Nanoscience, Delft University of Technology, Lorentzweg 1, 2628 CJ Delft, The Netherlands*
[2] *Instituto Ciencia Molecular (ICMol), Univ. Valencia, C/Catedrático José Beltrán 2, E-46980, Paterna, Spain*
[3] *Departamento de Física de la Materia Condensada (C–III). Universidad Autónoma de Madrid, Campus de Cantoblanco, 28049 Madrid, Spain*
[4] *Instituto Madrileño de Estudios Avanzados en Nanociencia IMDEA-Nanociencia, E-28049 Madrid, Spain*

Received: 11 December 2012
Revised: 15 January 2013
Accepted: 17 January 2013

© Tsinghua University Press and Springer-Verlag Berlin Heidelberg 2013

KEYWORDS

atomically thin layer,
metal dichalcogenide,
layered superconductor,
$TaSe_2$,
optical microscopy,
Raman spectroscopy

ABSTRACT

Deposition of clean and defect-free atomically thin two-dimensional crystalline flakes on surfaces by mechanical exfoliation of layered bulk materials has proven to be a powerful technique, but it requires a fast, reliable and non-destructive way to identify the atomically thin flakes among a crowd of thick flakes. In this work, we provide general guidelines to identify ultrathin flakes of $TaSe_2$ by means of optical microscopy and Raman spectroscopy. Additionally, we determine the optimal substrates to facilitate the optical identification of atomically thin $TaSe_2$ crystals. Experimental realization and isolation of ultrathin layers of $TaSe_2$ enables future studies on the role of the dimensionality in interesting phenomena such as superconductivity and charge density waves.

1 Introduction

Experimental isolation of graphene by mechanical exfoliation [1] has unleashed interest in a whole family of atomically thin materials which exhibit a variety of interesting properties ranging from topological insulator behavior to superconductivity [2–15]. Only a few two-dimensional (2D) crystals have been fabricated and thoroughly characterized [16–20], and most of the other possible 2D crystals with attractive properties remain barely explored. For instance, layered transition metal dichalcogenides with the formula MX_2 (M = Mo,

Address correspondence to Andres Castellanos-Gomez, a.castellanosgomez@tudelft.nl; Gabino Rubio-Bollinger, gabino.rubio@uam.es

W, Nb, Ta or Ti and X = Se, S or Te) present a broad variety of electrical properties ranging from wide band-gap semiconductors to superconductors. As in the case of graphene, while fabrication by mechanical exfoliation from bulk crystals of these layered materials is rather simple [2], identification of atomically thin flakes requires fast, reliable and non-destructive characterization techniques [21–27].

The realization of ultrathin superconducting layers would enable one to employ the electric field effect to control physical properties such as the superconducting transition temperature or to study the interplay between the superconductivity and the sample dimensionality. However, among the family of transition metal dichalcogenides, studies of atomically thin superconducting layers are scarce and mainly focused on $NbSe_2$ and TaS_2 crystals [3, 4, 28]. $TaSe_2$ is a good example of a layered material which has not been studied in its atomically thin form so far, while it is very interesting. In fact, in its bulk form, $TaSe_2$ is among the most studied charge density wave (CDW) systems as it shows both incommensurate and commensurate density-wave phases and a superconducting transition below 0.15 K [29, 30].

In this work, we report the fabrication of atomically thin two-dimensional $TaSe_2$ crystals on SiO_2/Si wafers. We perform a combined characterization by atomic force microscopy (AFM), quantitative optical microscopy and Raman spectroscopy. We also determine the optimal SiO_2 thickness to optically identify ultrathin $TaSe_2$ crystals. This work constitutes a necessary step towards further studies on other properties of atomically thin $TaSe_2$ sheets.

2 Experimental

Starting elemental materials were used as received from commercial suppliers with no further purification.

2.1 $TaSe_2$ single-crystal fabrication

$TaSe_2$ crystals were synthesized from the elemental components in a two-step process. Firstly, polycrystalline $TaSe_2$ was obtained by ceramic combination of stoichiometric ratios of Ta and Se. Ta powder, 99.99% trace metals basis and Se powder, −100 mesh, 99.99% trace metals basis were used. Powdered starting materials were intimately mixed, placed inside an evacuated quartz ampoule and reacted at 900 °C for 9 days. The resulting free-flowing glittery grey microcrystals were then transformed into large single-crystals using the chemical vapor transport (CVT) methodology. For that purpose, 1 g of $TaSe_2$ polycrystalline material together with 275 mg of I_2 were loaded into a 500 mm long quartz ampoule (OD: 18 mm, wall-thickness: 1.5 mm). The mixture was placed at one end of the ampoule which was exhaustively evacuated and flame-sealed. The quartz tube was finally placed inside a three-zone split muffle where a gradient of 25 °C was established between the leftmost load (725 °C) and central growth (700 °C) zones. A gradient of 25 °C was also set between the rightmost and central regions. The temperature gradient was maintained constant during 15 days and the muffle was eventually switched off and left to cool down to ambient conditions. Millimetric $TaSe_2$ crystals were recovered from the ampoule's central zone, exhaustively rinsed with diethyl ether and stored under a N_2 atmosphere.

2.2 Viscoelastic-stamp based exfoliation

The viscoelastic stamps employed during the $TaSe_2$ micromechanical exfoliation were based on poly (dimethylsiloxane) (PDMS) stamps, a viscoelastic material commonly used in microimprint lithography. The PDMS stamps were cast by curing the Sylgard® 184 elastomer kit purchased from Dow Corning [26].

2.3 Atomic force microscopy

AFM was used to characterize the thickness of the fabricated flakes. A Nanotec Cervantes AFM (Nanotec Electronica) was operated in contact mode under ambient conditions. We selected contact mode AFM instead of dynamic modes of operation to avoid artifacts in the determination of the flake thickness [31]. The piezoelectric actuators of the AFM have been calibrated by means of a recently developed calibration method to provide a determination of the flake thickness as accurate as possible [32].

2.4 Optical microscopy

The quantitative measurements of the optical contrast

of ultrathin $TaSe_2$ flakes were carried out with a Nikon Eclipse LV100 optical microscope under normal incidence with a 50× objective (numerical aperture NA = 0.55) and with a digital camera EO-1918C 1/1.8″ (from Edmund Optics) attached to the microscope trinocular. The illumination wavelength was selected by means of nine narrow band-pass filters (10 nm full width at half maximum FWHM) with central wavelengths 450 nm, 500 nm, 520 nm, 546 nm, 568 nm, 600 nm, 632 nm, 650 nm and 694 nm purchased from Edmund Optics.

2.5 Raman spectroscopy

A micro-Raman spectrometer (Renishaw in Via RM 2000) was used in a backscattering configuration excited with a visible laser light (λ = 514 nm) to characterize the ultrathin $TaSe_2$ layers. The spectra were collected through a 100× objective and recorded with 1,800 lines/mm grating providing the spectral resolution of ~1 cm^{-1}.

3 Results and discussion

Ultrathin two-dimensional crystals were fabricated from bulk 2H-$TaSe_2$ crystals, grown by a chemical vapor growth method (see the Experimental section), using a variation of the graphene micromechanical cleavage method [2]. As previously demonstrated for other layered crystals, adhesive-free exfoliation of bulk crystals can be performed with viscoelastic silicone stamps [12, 26, 33]. The surface of the stamp containing $TaSe_2$ crystals was pressed against another clean stamp and peeled off rapidly to re-cleave the crystals. This maneuver was repeated several times until only faint atomically thin flakes were observed on the surface of the stamp by optical microscopy. As a final step, the crystals were transferred to an oxidized silicon wafer (300 nm thick oxide) by slightly pressing the silicone stamp against the wafer surface and subsequently peeling it off slowly. The advantage of the silicone stamp over the Scotch tape method is that one can avoid leaving adhesive traces on the wafer surface preventing the contamination of the flakes and the cantilever tip used in AFM studies of the samples [34]. In addition we have not found differences in the obtained flakes, neither their minimal thickness nor their size, when transferred using the silicone stamp or the commonly used Scotch tape method.

Inspection of the samples under an optical microscope enables quick identification of the flakes and their size. In addition, it is possible to get a rough estimate of the thickness of the flakes due to a light interference effect owing to the presence of the thin silicon oxide layer which makes their color thickness-dependent under white light illumination (this effect is usually referred to as interference color) [35]. Typically, the obtained flakes with thicknesses below 40 nm are several microns wide (see Fig. 1). Selected flakes were analyzed with an AFM operated in contact mode to

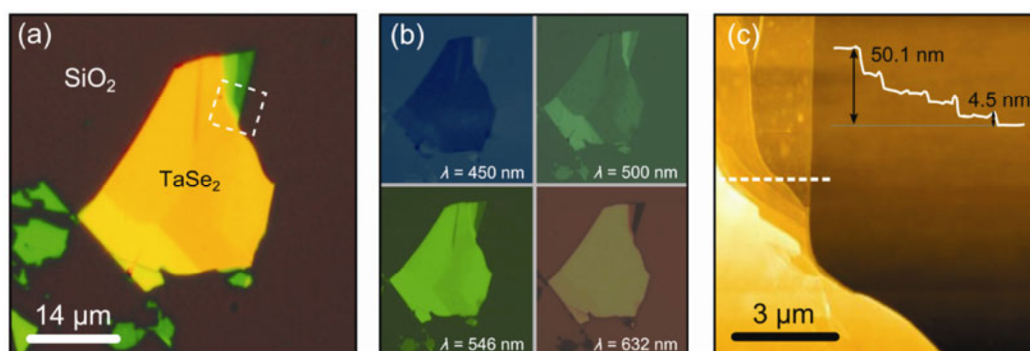

Figure 1 Optical and atomic force microscopy images of $TaSe_2$ nanosheets: (a) optical micrograph under white illumination of $TaSe_2$ flakes deposited on a 300 nm SiO_2/Si substrate; (b) different optical micrographs acquired at 450 nm, 500 nm, 546 nm and 632 nm by using narrow bandwidth filters; (c) AFM topography image of the region marked by a dashed rectangle in (a). A topographic line profile along the horizontal dashed line is inserted to indicate the thickness of the flakes. The root mean square roughness of the thinnest layer is 0.22 nm^2, while the roughness of the SiO_2 substrate is 0.20 nm^2. In some flakes the AFM topography shows a spike at the step edges, which could be attributed to rolling or folding during the deposition of the flake.

obtain topographic images. This allows for the accurate determination of their thickness with sub-nm resolution. The number of layers present in a selected flake was obtained by simply dividing the measured thickness by the $TaSe_2$ interlayer spacing 0.64 nm [36] (see Fig. 1(c) and Fig. S1 in the Electronic Supplementary Material (ESM)). Surprisingly, we found that $TaSe_2$ flakes just a few layers thick (5–15 layers) can be deposited by mechanical exfoliation and the yield rate is even higher than exfoliation of graphite (see the low magnification optical images of the fabricated samples in Fig. S2 in the ESM). However, we have not yet found single or bilayer (0.7 nm or 1.4 nm thick) $TaSe_2$ flakes, at least not large enough to allow for optical identification, presumably due to a subtle balance between the interactions at the viscoelastic stamp/$TaSe_2$, interlayer $TaSe_2$ and $TaSe_2$/SiO_2 interfaces. Nevertheless, the expected optical contrast for a single layer $TaSe_2$ would be around –0.1 (see Fig. 3 and Fig. S5 in the ESM) for an optimal SiO_2 substrate thickness, and therefore it would be easily identifiable.

A quantitative method to determine the thickness of thin $TaSe_2$ flakes through optical microscopy would provide a fast alternative to AFM, which is a very slow technique. In this study, we have quantitatively studied the optical contrast (C), which depends on the flake thickness (d) and the illumination wavelength (λ):

$$C(d_1,\lambda)=\frac{I_{\text{flake}}-I_{\text{substrate}}}{I_{\text{flake}}+I_{\text{substrate}}} \tag{1}$$

where I_{flake} and $I_{\text{substrate}}$ are the reflected light intensities from the flake and the SiO_2 substrate, respectively. The measured contrast is compared to the contrast calculated using a model based on Fresnel's laws, which accounts for the light intensity reflected either from the substrate or from the flake [22]:

$$I_{\text{substrate}}(d_1,\lambda)=\left|\frac{r_{02}+r_{23}\mathrm{e}^{-2\mathrm{i}\Phi_2}}{1+r_{02}r_{23}\mathrm{e}^{-2\mathrm{i}\Phi_2}}\right|^2 \tag{2}$$

$$I_{\text{flake}}(d_1,\lambda)=$$
$$\left|\frac{r_{01}\mathrm{e}^{\mathrm{i}(\Phi_1+\Phi_2)}+r_{12}\mathrm{e}^{-\mathrm{i}(\Phi_1-\Phi_2)}+r_{23}\mathrm{e}^{-\mathrm{i}(\Phi_1+\Phi_2)}+r_{01}r_{12}r_{23}\mathrm{e}^{\mathrm{i}(\Phi_1-\Phi_2)}}{\mathrm{e}^{\mathrm{i}(\Phi_1+\Phi_2)}+r_{01}r_{12}\mathrm{e}^{-\mathrm{i}(\Phi_1-\Phi_2)}+r_{01}r_{23}\mathrm{e}^{-\mathrm{i}(\Phi_1+\Phi_2)}+r_{12}r_{23}\mathrm{e}^{\mathrm{i}(\Phi_1-\Phi_2)}}\right|^2$$

where the subindices 0, 1, 2 and 3 label the different media (air, $TaSe_2$, SiO_2 and Si respectively), $\tilde{n}_j(\lambda)=n_j-\mathrm{i}\kappa_j$ is the complex refractive index of the medium j, d_j is the thickness of medium j, $\Phi_j=2\pi\tilde{n}_jd_j/\lambda$ is the phase shift introduced by the medium j and $r_{jk}=(\tilde{n}_j-\tilde{n}_k)/(\tilde{n}_j+\tilde{n}_k)$ is the amplitude of the reflected path in the interface between the media j and k.

We have analyzed the optical contrast of 30 flakes with thicknesses ranging from 3 to 36 nm (~4 to 56 layers), under a well-defined illumination wavelength using narrowband optical filters (see Fig. 1(b)) spanning the visible spectrum (see the Experimental section). The measured optical contrast is shown in Fig. 2, and accurately follows Eqs. (1) and (2) using the wavelength-dependent complex refractive index reported in Ref. [37] for bulk 2H-$TaSe_2$ crystals (see Fig. S3 in the ESM). The quantitative analysis of the optical contrast of the flakes under different illumination wavelengths provides a fast and reliable way to discriminate atomically thin flakes from thicker flakes. For instance, flakes thinner than 12 nm

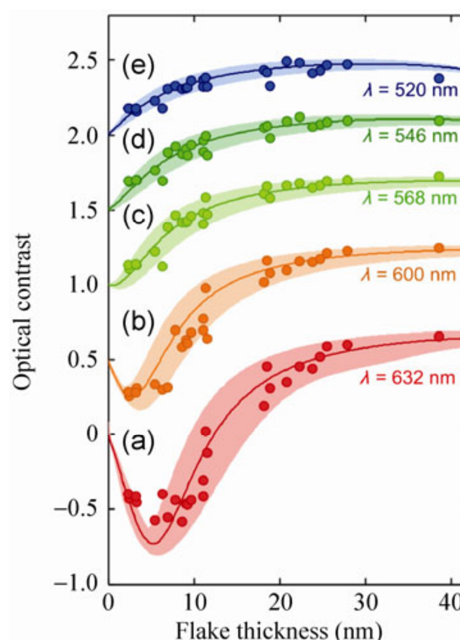

Figure 2 Measured optical contrast (circles) of the $TaSe_2$ flakes as a function of their thickness under the following illumination wavelengths: (a) 632 nm (red), (b) 600 nm (orange), (c) 568 nm (light green), (d) 546 nm (green) and (e) 520 nm (blue). The contrast values have been shifted 0.5, 1.0, 1.5 and 2.0 for (b), (c), (d) and (e), respectively. The solid lines correspond to the expected contrasts derived from Eqs. (1) and (2) using the wavelength-dependent complex refractive index reported in the literature [29] and considering a possible variation in n and κ of 10 % (indicated by a shadow area around the solid line).

(~20 layers) present a negative contrast for λ = 632 nm while thicker flakes have a positive contrast. Furthermore, flakes thinner than 6 nm (9–10 layers) can be distinguished from the rest because of their negative contrast for λ = 600 nm.

To determine the best SiO_2/Si substrate to identify ultrathin $TaSe_2$ layers, the optical contrast of a single-layer $TaSe_2$ layer has been calculated as a function of the illumination wavelength and the SiO_2 thickness (Fig. 3(a)). We define as optimal substrates for the optical identification those with a SiO_2 thickness that optimizes the contrast for λ = 550 nm, which is the illumination wavelength to which the human eye has maximum sensitivity [38]. For instance, substrates with a SiO_2 capping layer of 80 nm (–27% contrast, nearly λ-independent) and 265 nm (–27% contrast at λ = 550 nm) optimize the optical identification of nanolayers of $TaSe_2$. In the widespread work on graphene in nanofabrication laboratories however, it is more common to find wafers with 285 nm and 90 nm SiO_2 thickness (which are optimized to identify graphene). Although these thicknesses are not optimal, one can identify ultrathin $TaSe_2$ flakes on those substrates. Figures 3(b) and 3(c) show the calculated optical contrast for $TaSe_2$ layers as a function of their thickness and the illumination wavelength for these two commonly used SiO_2/Si substrates (90 nm and 285 nm of SiO_2 thickness). In Fig. S5 (in the ESM) we also present Figs. 3(b) and 3(c) recalculated for SiO_2 substrates that optimize the optical identification of $TaSe_2$ nanosheets (80 nm and 265 nm of SiO_2).

Raman spectroscopy can be considered as an alternative and complementary fast, reliable and non-destructive technique to identify ultrathin $TaSe_2$ layers. Indeed, Raman spectroscopy has been successfully employed to characterize the thickness of several atomically thin materials such as graphene [21, 39] and MoS_2 [40–42]. Nevertheless, this technique has proven to be ineffective to detect ultrathin layers of mica [12] and, moreover, other 2D materials (such as atomically thin $NbSe_2$) are significantly damaged during the Raman spectroscopy measurements [4]. It is therefore necessary to investigate whether Raman microscopy can be employed to detect and to determine the thickness of ultrathin $TaSe_2$ layers.

Figure 4(a) shows the Raman spectra measured for $TaSe_2$ flakes with thicknesses ranging from four layers to more than 40 layers. The spectra show five prominent peaks around 150 cm^{-1}, 208 cm^{-1}, 235 cm^{-1} and 519 cm^{-1} and show the characteristic features of 2H-$TaSe_2$

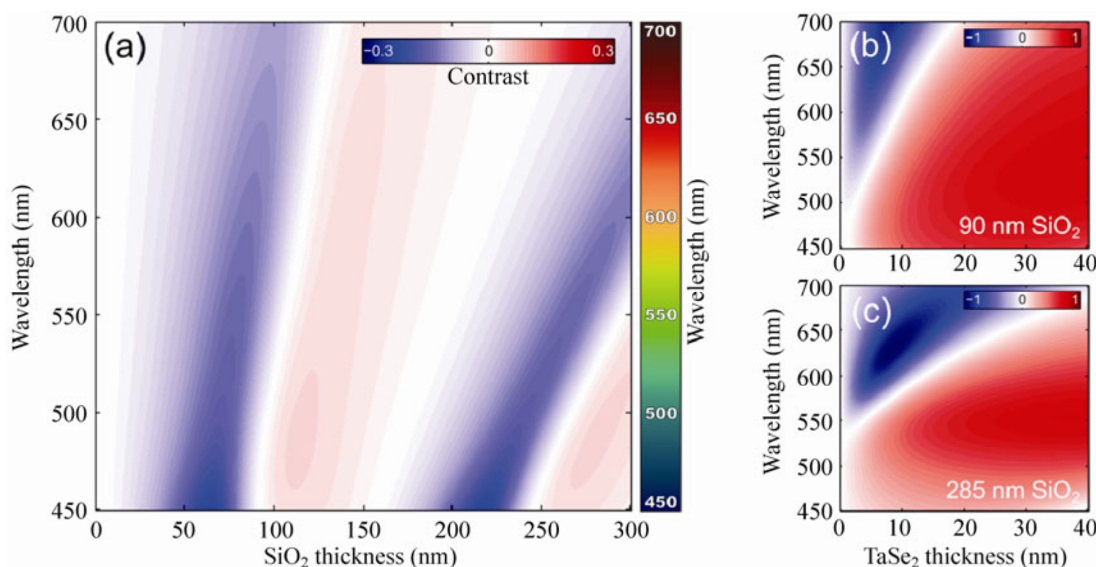

Figure 3 (a) Calculated optical contrast colormap for a single layer of $TaSe_2$ (0.64 nm thick) as a function of the illumination wavelength and SiO_2 thickness derived from Eqs. (1) and (2) and the complex refractive index reported for bulk 2H-$TaSe_2$ [16]. A correspondence between the apparent color and the illumination wavelength is shown in the colorbar at the right side of (a). The calculated optical contrast as a function of the wavelength and the $TaSe_2$ thicknesses for substrates with (b) 90 nm and (c) 285 nm SiO_2 thickness (which are rather standard to fabricate other 2D crystals such as graphene).

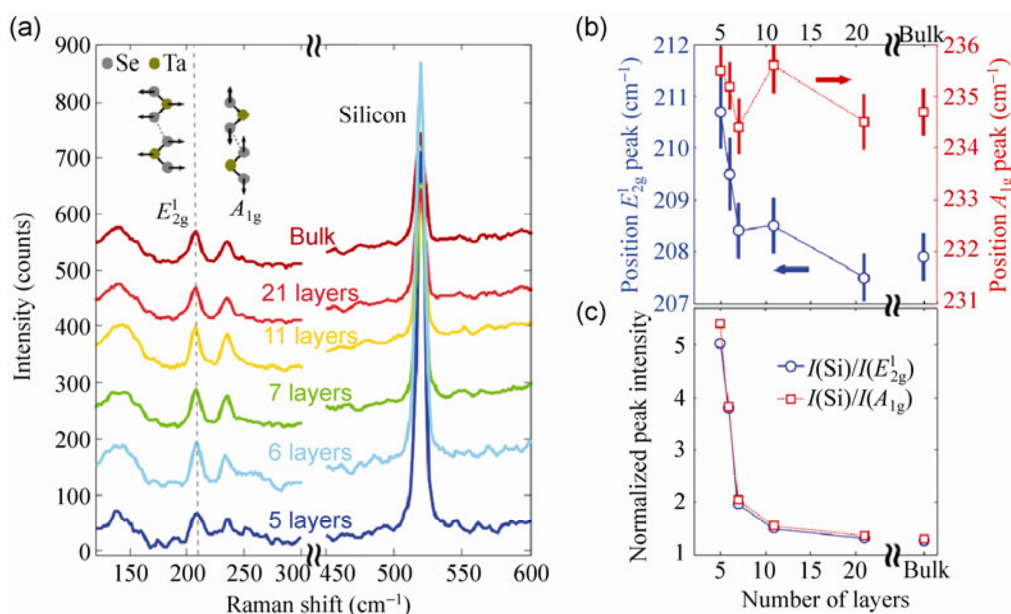

Figure 4 (a) Raman spectra of $TaSe_2$ flakes with thicknesses ranging from five layers to >40 layers (bulk). (b) Position of the E^1_{2g} and A_{1g} Raman modes. (c) Ratio between the maximum intensities of the silicon and the E^1_{2g} and A_{1g} peaks.

[43, 44]. The Raman peak near 150 cm^{-1} is due to a two-phonon scattering process [43, 44]. The peak around 208 cm^{-1} (labelled E^1_{2g}) corresponds to the excitation of a vibrational mode in which the Se and Ta atoms oscillate, in anti-phase, parallel to the crystal surface. The peak around 235 cm^{-1} (labelled A_{1g}), on the other hand, is due to the vibration of the Se atoms, in anti-phase, perpendicularly to the crystal surface while the Ta atoms are fixed [43, 44]. Finally, the peak at 519 cm^{-1} is due to the vibration of the lattice of the silicon substrate underneath.

The position of the E^1_{2g} and A_{1g} peaks as a function of the $TaSe_2$ layer thickness is presented in Fig. 4(b). Within a classical model for coupled harmonic oscillators [45], both the E^1_{2g} and A_{1g} modes are expected to shift to lower frequencies as the number of layers decreases because the interlayer van der Waals interaction decreases and so does the effective restoring forces acting on the atoms. However, we observed that the E^1_{2g} peak shifts to higher frequencies as the number of layers decreases and the position of the A_{1g} peak shows no clear shift within the experimental resolution, in agreement with previous experiments on intercalated $TaSe_2$ samples [44]. Similar shifts of the E^1_{2g} peak have also been observed for another transition metal dichalcogenide, MoS_2, and were explained by an enhancement of the dielectric screening of the long-range Coulomb interaction between the effective charges with increasing number of layers, which reduces the overall restoring force on the atoms [46].

The monotonic thickness dependence of the E^1_{2g} peak position can be employed to determine the number of layers of $TaSe_2$ flakes, as has been previously employed for other materials such as MoS_2 [40, 42]. The signal-to-noise ratio of this frequency shift, however, would make this determination rather inaccurate for flakes thinner than 7 layers (1–2 layers of uncertainty) and even impractical for thicker flakes. Nevertheless, as for other dichalcogenides (such as MoS_2) [6], the E^1_{2g} shift may be even larger for single and bilayer $TaSe_2$ thus helping to identify them. An alternative procedure to determine the number of layers of $TaSe_2$ flakes relies on measuring the ratio between the intensities of the silicon peak and the E^1_{2g} and A_{1g} peaks [47]. Figure 4(c) shows that I(Si)/I(E^1_{2g}) and I(Si)/I(A_{1g}) vary monotonically and strongly with the number of layers. The thickness of flakes thinner than 20 layers can be determined with an uncertainty of less than one layer. Notice that for substrates with

a different SiO_2 thickness, the thickness dependence of the ratios $I(Si)/I(E^1_{2g})$ and $I(Si)/I(A_{1g})$ will be different but after a calibration measurement (as in Fig. 4(c)) they can be used to accurately determine the number of layers of $TaSe_2$ flakes.

To avoid laser-induced modification of the samples [48], all spectra were recorded with a power level P in the range 0.5–1 mW and an accumulation time of 1 s. Interestingly, we found that the laser-induced damage of $TaSe_2$ flakes can be monitored by measuring their Raman spectra. Figure 5 shows the Raman spectra of a five-layer $TaSe_2$ flake measured using 1 s (blue line) and 2 s (red line) accumulation times. When an accumulation time of 2 s was employed, both the Raman spectrum and the topography of the flake demonstrate that the flake is modified, possibly due to laser-induced oxidization. A peak around 260 cm^{-1} appears concomitantly with the laser-induced modification of the topography of the $TaSe_2$ flake. Therefore, the appearance of this peak can be used to regulate the laser intensity in order to avoid laser-induced oxidation of the flakes.

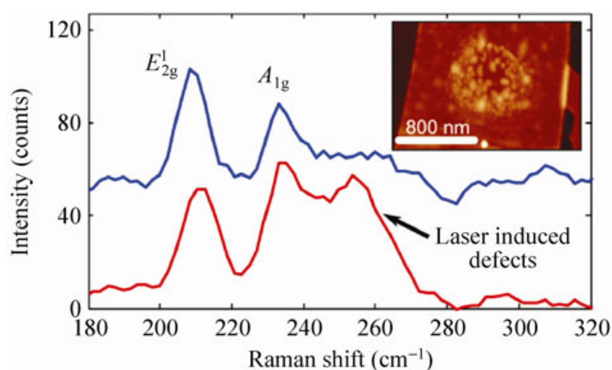

Figure 5 Raman spectra of a $TaSe_2$ flake with five layers measured with accumulation times of 1 s (blue line) and 2 s (red line). (Inset) Atomic force microscopy topography image of the flake after acquisition of the Raman spectrum for 2 s, showing that the layer has been modified by the laser beam.

4 Conclusions

Atomically thin $TaSe_2$ sheets have been fabricated by mechanical exfoliation of bulk 2H-$TaSe_2$ single crystals grown by a chemical vapor transport method. We have demonstrated that optical microscopy and Raman spectroscopy can be used to identify atomically thin $TaSe_2$ crystals and to distinguish them from thicker crystals. The optimal SiO_2 thickness to facilitate the optical identification of these atomically thin flakes on SiO_2/Si wafers has been also calculated. Additionally, we have demonstrated that Raman spectroscopy can be used to identify ultrathin $TaSe_2$ flakes and to monitor any possible laser-induced damage. This work can thus be considered as a necessary first step towards the deeper study of ultrathin $TaSe_2$.

Acknowledgements

This work was supported by the Spanish MICINN/MINECO (projects MAT2011-25046, MAT2011-22785 and CONSOLIDER-INGENIO-2010 on Nanociencia Molecular, CSD-2007-00010), the Comunidad de Madrid (program Nanobiomagnet S2009/MAT-1726), the Generalidad Valenciana (PROMETEO and ISIC programs) and the European Union (Projects RODIN and ELFOS).

Electronic Supplementary Material: Supplementary material is available in the online version of this article at http://dx.doi.org/10.1007/s12274-013-0295-9.

References

[1] Novoselov, K. S.; Geim, A. K.; Morozov, S. V.; Jiang, D.; Zhang, Y.; Dubonos, S. V.; Grigorieva, I. V.; Firsov, A. A. Electric field effect in atomically thin carbon films. *Science* **2004**, *306*, 666–669.

[2] Novoselov, K. S.; Jiang, D.; Schedin, F.; Booth, T. J.; Khotkevich, V. V.; Morozov, S. V.; Geim, A. K. Two-dimensional atomic crystals. *Proc. Natl. Acad. Sci. USA* **2005**, *102*, 10451–10453.

[3] Ayari, A.; Cobas, E.; Ogundadegbe, O.; Fuhrer, M. S. Realization and electrical characterization of ultrathin crystals of layered transition-metal dichalcogenides. *J. Appl. Phys.* **2007**, *101*, 014507.

[4] Staley, N. E.; Wu, J.; Eklund, P.; Liu, Y.; Li, L. J.; Xu, Z. Electric field effect on superconductivity in atomically thin flakes of $NbSe_2$. *Phys. Rev. B* **2009**, *80*, 184505.

[5] Khan, J.; Nolen, C. M.; Teweldebrhan, D.; Wickramaratne, D.; Lake, R. K.; Balandin, A. A. Anomalous electron transport in back-gated field-effect transistors with $TiTe_2$ semimetal thin-film channels. *Appl. Phys. Lett.* **2012**, *100*, 043109.

[6] Lee, C.; Yan, H.; Brus, L. E.; Heinz, T. F.; Hone, J.; Ryu, S. Anomalous lattice vibrations of single- and few-layer MoS_2. *ACS Nano* **2010**, *4*, 2695–2700.

[7] Teweldebrhan, D.; Goyal, V.; Rahman, M.; Balandin, A. A. Atomically-thin crystalline films and ribbons of bismuth telluride. *Appl. Phys. Lett.* **2010**, *96*, 053107.

[8] Dean, C. R.; Young, A. F.; Meric, I.; Lee, C.; Wang, L.; Sorgenfrei, S.; Watanabe, K.; Taniguchi, T.; Kim, P.; Shepard, K. L.; et al. Boron nitride substrates for high-quality graphene electronics. *Nat. Nanotechnol.* **2010**, *5*, 722–726.

[9] Splendiani, A.; Sun, L.; Zhang, Y.; Li, T.; Kim, J.; Chim, C.-Y.; Galli, G.; Wang, F. Emerging photoluminescence in monolayer MoS_2. *Nano Lett.* **2010**, *10*, 1271–1275.

[10] Ramakrishna Matte, H. S. S.; Gomathi, A.; Manna, A. K.; Late, D. J.; Datta, R.; Pati, S. K.; Rao, C. N. R. MoS_2 and WS_2 analogues of graphene. *Angew. Chem. Int. Ed.* **2010**, *49*, 4059–4062.

[11] Radisavljevic, B.; Radenovic, A.; Brivio, J.; Giacometti, V.; Kis, A. Single-layer MoS_2 transistors. *Nat. Nanotechnol.* **2011**, *6*, 147–150.

[12] Castellanos-Gomez, A.; Wojtaszek, M.; Tombros, N.; Agraït, N.; van Wees, B. J.; Rubio-Bollinger, G. Atomically thin mica flakes and their application as ultrathin insulating substrates for graphene. *Small* **2011**, *7*, 2491–2497.

[13] Castellanos-Gomez, A.; Poot, M.; Amor-Amorós, A.; Steele, G.; van der Zant, H.; Agraït, N.; Rubio-Bollinger, G. Mechanical properties of freely suspended atomically thin dielectric layers of mica. *Nano Res.* **2012**, *5*, 550–557.

[14] Castellanos-Gomez, A.; Poot, M.; Steele, G. A.; van der Zant, H. S. J.; Agraït, N.; Rubio-Bollinger, G. Elastic properties of freely suspended MoS_2 nanosheets. *Adv. Mater.* **2012**, *24*, 772–775.

[15] Yin, Z. Y.; Li, H.; Li, H.; Jiang, L.; Shi, Y. M.; Sun, Y. H.; Lu, G.; Zhang, Q.; Chen, X. D.; Zhang, H. Single-layer MoS_2 phototransistors. *ACS Nano* **2012**, *6*, 74–80.

[16] Zhan, Y. J.; Liu, Z.; Najmaei, S.; Ajayan, P. M.; Lou, J. Large-area vapor-phase growth and characterization of MoS_2 atomic layers on a SiO_2 substrate. *Small* **2012**, *8*, 966–971.

[17] Zeng, Z. Y.; Yin, Z. Y.; Huang, X.; Li, H.; He, Q. Y.; Lu, G.; Boey, F.; Zhang, H. Single-layer semiconducting nanosheets: High-yield preparation and device fabrication. *Angew. Chem. Int. Ed.* **2011**, *50*, 11093–11097.

[18] Zeng, Z. Y.; Sun, T.; Zhu, J. X.; Huang, X.; Yin, Z. Y.; Lu, G.; Fan, Z. X.; Yan, Q. Y.; Hng, H. H.; Zhang, H. An effective method for the fabrication of few-layer-thick inorganic nanosheets. *Angew. Chem. Int. Ed.* **2012**, *51*, 9052–9056.

[19] Liu, K.-K.; Zhang, W. J.; Lee, Y.-H.; Lin, Y.-C.; Chang, M.-T.; Su, C.-Y.; Chang, C.-S.; Li, H.; Shi, Y. M.; Zhang, H.; et al. Growth of large-area and highly crystalline MoS_2 thin layers on insulating substrates. *Nano Lett.* **2012**, *12*, 1538–1544.

[20] Li, H.; Lu, G.; Wang, Y. L.; Yin, Z. Y.; Cong, C. X.; He, Q. Y.; Wang, L.; Ding, F.; Yu, T.; Zhang, H. Mechanical exfoliation and characterization of single- and few-layer nanosheets of WSe_2, TaS_2, and $TaSe_2$. *Small*, in press, DOI: 10.1002/smll.201202919.

[21] Ferrari, A. C.; Meyer, J. C.; Scardaci, V.; Casiraghi, C.; Lazzeri, M.; Mauri, F.; Piscanec, S.; Jiang, D.; Novoselov, K. S.; Roth, S.; et al. Raman spectrum of graphene and graphene layers. *Phys. Rev. Lett.* **2006**, *97*, 187401.

[22] Blake, P.; Hill, E. W.; Neto, A. H. C.; Novoselov, K. S.; Jiang, D.; Yang, R.; Booth, T. J.; Geim, A. K. Making graphene visible. *Appl. Phys. Lett.* **2007**, *91*, 063124.

[23] Casiraghi, C.; Hartschuh, A.; Lidorikis, E.; Qian, H.; Harutyunyan, H.; Gokus, T.; Novoselov, K. S.; Ferrari, A. C. Rayleigh imaging of graphene and graphene layers. *Nano Lett.* **2007**, *7*, 2711–2717.

[24] Jung, I.; Pelton, M.; Piner, R.; Dikin, D. A.; Stankovich, S.; Watcharotone, S.; Hausner, M.; Ruoff, R. S. Simple approach for high-contrast optical imaging and characterization of graphene-based sheets. *Nano Lett.* **2007**, *7*, 3569–3575.

[25] Roddaro, S.; Pingue, P.; Piazza, V.; Pellegrini, V.; Beltram, F. The optical visibility of graphene: Interference colors of ultrathin graphite on SiO_2. *Nano Lett.* **2007**, *7*, 2707–2710.

[26] Castellanos-Gomez, A.; Agraït, N.; Rubio-Bollinger, G. Optical identification of atomically thin dichalcogenide crystals. *Appl. Phys. Lett.* **2010**, *96*, 213116.

[27] Li, H.; Lu, G.; Yin, Z. Y.; He, Q. Y.; Zhang, Q.; Zhang, H. Optical identification of single-and few-layer MoS_2 Sheets. *Small* **2012**, *8*, 682–686.

[28] Sengupta, S.; Solanki, H. S.; Singh, V.; Dhara, S.; Deshmukh, M. M. Electromechanical resonators as probes of the charge density wave transition at the nanoscale in $NbSe_2$. *Phys. Rev. B* **2010**, *82*, 155432.

[29] Leininger, P.; Chernyshov, D.; Bosak, A.; Berger, H.; Inosov, D. S. Competing charge density waves and temperature-dependent nesting in 2H-$TaSe_2$. *Phys. Rev. B* **2011**, *83*, 233101.

[30] Galvis, J. A.; Rodière, P.; Guillamón, I.; Osorio, M. R.; Rodrigo, J. G.; Cario, L.; Navarro-Moratalla, E.; Coronado, E.; Vieira, S.; Suderow, H. Flat band in superconducting layers of 2H-$TaSe_2$. arXiv:1210.2659.

[31] Nemes-Incze, P.; Osváth, Z.; Kamarás, K.; Biró, L. P. Anomalies in thickness measurements of graphene and few layer graphite crystals by tapping mode atomic force microscopy. *Carbon* **2008**, *46*, 1435–1442.

[32] Castellanos-Gomez, A.; Arroyo, C. R.; Agraït, N.; Rubio-Bollinger, G. Calibration of piezoelectric positioning actuators using a reference voltage-to-displacement transducer based on quartz tuning forks. *Microsc. Microanal.* **2012**, *18*, 353–358.

[33] Moreno-Moreno, M.; Castellanos-Gomez, A.; Rubio-Bollinger, G.; Gomez-Herrero, J.; Agraït, N. Ultralong natural graphene nanoribbons and their electrical conductivity. *Small* **2009**, *5*, 924–927.

[34] Moser, J.;Verdaguer, A.; Jiménez, D.; Barreiro, A.; Bachtold, A. The environment of graphene probed by electrostatic force microscopy. *Appl. Phys. Lett.* **2008**, *92*, 123507.

[35] Kvavle, J.; Bell, C.; Henrie, J.; Schultz, S.; Hawkins, A. Improvement to reflective dielectric film color pictures. *Opt. Express* **2004**, *12*, 5789–5794.

[36] McWhan, D. B.; Fleming, R. M.; Moncton, D. E.; DiSalvo, F. J. Reentrant lock-in transition of the charge-density wave in 2H-$TaSe_2$ at high pressure. *Phys. Rev. Lett.* **1980**, *45*, 269–272.

[37] Beal, A. R.; Hughes, H. P.; Liang, W. Y. The reflectivity spectra of some group *VA* transition metal dichalcogenides. *J. Phys. C Solid State Phys.* **1975**, *8*, 4236.

[38] Wald, G. Human vision and the spectrum. *Science* **1945**, *101*, 653–658.

[39] Graf, D.; Molitor, F.; Ensslin, K.; Stampfer, C.; Jungen, A.; Hierold, C.; Wirtz, L. Spatially resolved Raman spectroscopy of single-and few-layer graphene. *Nano Lett.* **2007**, *7*, 238–242.

[40] Mak, K. F.; Lee, C.; Hone, J.; Shan, J.; Heinz, T. F. Atomically thin MoS_2: A new direct-gap semiconductor. *Phys. Rev. Lett.* **2010**, *105*, 136905.

[41] Korn, T.; Heydrich, S.; Hirmer, M.; Schmutzler, J.; Schüller, C. Low-temperature photocarrier dynamics in monolayer MoS_2. *Appl. Phys. Lett.* **2011**, *99*, 102109.

[42] Mak, K. F.; Lee, C.; Hone, J.; Shan, J.; Heinz, T. F. Atomically thin MoS_2: A new direct-gap semiconductor. *Phys. Rev. Lett.* **2010**, *105*, 136805.

[43] Holy, J. A.; Klein, M. V.; McMillan, W. L.; Meyer, S. F. Raman-active lattice vibrations of the commensurate superlattic in 2H-$TaSe_2$. *Phys. Rev. Lett.* **1976**, *37*, 1145–1148.

[44] Tsang, J.; Shafer, M. Raman spectroscopy of intercalated layered structure compounds. *Solid State Commun.* **1978**, *25*, 999–1002.

[45] Li, T.; Galli, G. Electronic Properties of MoS_2 Nanoparticles. *J. Phys. Chem. C* **2007**, *111*, 16192–16196.

[46] Molina-Sánchez, A.; Wirtz, L. Phonons in single-layer and few-layer MoS_2 and WS_2. *Phys. Rev. B* **2011**, *84*, 155413.

[47] Koh, Y. K.; Bae, M. H.; Cahill, D. G.; Pop, E. Reliably counting atomic planes of few-layer graphene ($n > 4$). *ACS Nano* **2011**, *5*, 269–274.

[48] Castellanos-Gomez, A.; Barkelid, M.; Goossens, A. M.; Calado, V. E.; van der Zant, H. S. J.; Steele, G. A. Laser-thinning of MoS_2: On demand generation of a single-layer semiconductor. *Nano Lett.* **2012**, *12*, 3187–3192.